IPFR

Institute of Plasma and Fusion Research

E × B INSTABILITY IN REGIONS OF STRONG ELECTRIC SHEAR

Francis F. Chen
Electrical Engineering Department
and
Institute of Plasma and Fusion Research
University of California, Los Angeles

Johannes Hsieh
University of Wisconsin

PPG – 1465

January 1993

Affiliated with the Departments of:

Astronomy
Earth and Space Sciences
Electrical Engineering
Materials Science and Engineering
Mechanical, Aerospace and Nuclear Engineering
Physics

and

Center for Advanced Accelerators
Institute of Geophysics and Planetary Physics

UNIVERSITY OF CALIFORNIA • LOS ANGELES

E × B INSTABILITY IN REGIONS OF STRONG ELECTRIC SHEAR

Francis F. Chen
Electrical Engineering Department
and
Institute of Plasma and Fusion Research
University of California, Los Angeles
Johannes Hsieh
University of Wisconsin

PPG – 1465 January 1993

This report was written for the *Proceedings of the International Workshop on Magnetic Turbulence and Transport in Magnetized Plasmas, Cargese, Corsica, 7/6-7/12/92.*

E × B INSTABILITY IN REGIONS OF STRONG ELECTRIC SHEAR

Francis F. Chen
University of California, Los Angeles, CA 90024-1594

Johannes Hsieh
University of Wisconsin, Madison, WI 53706-1687

Abstract

A magnetically confined plasma subject to a highly sheared electric field is found to be unstable to flute modes, even in the absence of collisions. Analysis of the instability is made without recourse to any assumption regarding the smallness of the ion gyroradius relative to the electric field shear length. The shape of the unstable mode is found by integrating over a plane slab. The perturbation tends, surprisingly, to peak near the "outside" of the plasma, where the density is low.

E × B INSTABILITY IN REGIONS OF STRONG ELECTRIC SHEAR

Francis F. Chen
University of California, Los Angeles, CA 90024-1594

Johannes Hsieh
University of Wisconsin, Madison, WI 53706-1687

I. Introduction

It is well known from the work of Simon [1] and Hoh [2] that a magnetized plasma in a transverse electric field suffers from a flute instability in the presence of ion-neutral collisions. The $E \times B$ drift of the ions is slowed down by neutral drag more than the electrons are, and the resulting charge separation when there is a density perturbation causes the perturbation to grow when the density and potential gradients are oppositely directed. This instability is normally observed in reflex discharges, and indeed is needed for the flow of the discharge current across the magnetic field. In a recent experiment by Sakawa [3], a similar instability was observed in a beam-generated plasma at such low pressures and weak magnetic fields that the Simon-Hoh mechanism could not have been operative. At the same time, the observed frequency was an order of magnitude smaller than both the $E \times B$ and diamagnetic drift frequencies, and was furthermore larger than the ion cyclotron frequency, thus eliminating all drift-wave mechanisms.

When the magnetic field is so weak that the plasma radius is much smaller than the ions' Larmor radii, but much larger than the electron Larmor radius, an $E \times B$ instability can occur even in a collisionless plasma because the ion and electron fluids drift around the cylindrical axis at different speeds. Because of the large ion orbits, small Larmor radius expansions fail, and the equilibrium is difficult to describe. By using model profiles for the potential and electric field distributions, we have been able to produce self-consistent profiles for the plasma density and ion drift velocity in both slab and cylindrical geometries. These results were given previously [4]; in this paper we present computations of the threshold and growth rate of the instability for the plane geometry case.

An instability of this type should be operative in the edge layer of an H-mode discharge in a tokamak, where the electric field is sharply sheared on a scale not much larger than an ion Larmor radius. The stability that is observed instead is not well understood, but may be related to the ion and electron drift profiles and their derivatives. The purpose of this paper is to suggest basic experiments on edge-layer instabilities which can be analyzed with self-consistently computed shear profiles.

II. Equilibrium profiles

Consider a slab of plasma $-L \leq x \leq L$, as shown in Fig. 1. In the presence of a magnetic field $B\hat{z}$, a potential $\phi(x)$ which increases monotonically with x will cause electrons to E × B drift in the $+y$ direction. The ions are assumed to be weakly magnetized, so that they move primarily in the $-x$ direction, but with a small but important velocity component in the y direction because of the curvature of their orbits. We assume an electric field of the form

$$\mathbf{E} = -(N/L)\,\phi_0\,\mathrm{sech}^2\,\xi\,\hat{\mathbf{x}} \quad , \tag{1}$$

which is derived from a potential of the form

$$\phi = \phi_0 \tanh \xi \quad , \tag{2}$$

where

$$\xi = Nx/L \quad . \tag{3}$$

By adjusting the parameter N, the sharpness of the E profile can be changed. The computations given here are for $N = 2$.

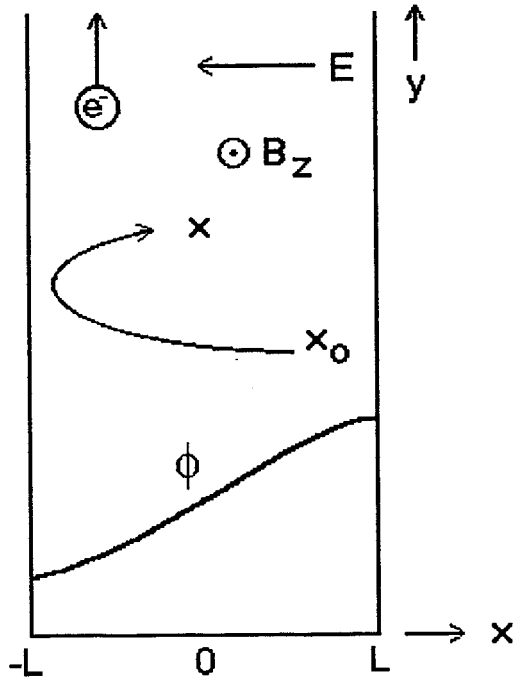

Figure 1: Diagram of the geometry assumed.

We postulate that ions are created at zero velocity by an unspecified mechanism at a rate $S(x)$, and that they are lost by ambipolar flow along the magnetic field to the ends of the plasma. The electrons form a neutralizing background with temperature T_0. Once the source function $S(x)$ and the electric field profile have been chosen, the plasma density is

uniquely determined. Consider an ion at position x which was born at position $x_0 > x$. Its total energy is given the potential drop between x and x_0; thus,

$$v^2(\xi, \xi_0) = (2e\phi_0/M)(\tanh\xi_0 - \tanh\xi) \quad . \tag{4}$$

The Lorentz force causes an acceleration in the y direction, given by

$$\frac{dv_y}{dt} = \frac{dv_y}{dx} v_x = -\Omega_c v_x \quad , \tag{5}$$

so that

$$v_y(\xi, \xi_0) = (L/N)\Omega_c(\xi_0 - \xi) \quad . \tag{6}$$

The x component of velocity is then given by

$$v_x^2(\xi, \xi_0) = v^2 - v_y^2 = (2e\phi/M)(\tanh\xi_0 - \tanh\xi) - (L\,\Omega_c/N)^2(\xi_0 - \xi)^2 \quad . \tag{7}$$

For ion confinement times much longer than their transit times across the slab, the flux nv_x is conserved, and the density can be computed by integrating the source $S(\xi_0)$ over all possible birth positions ξ_0, weighting the integral by the relative residence time $1/|v_x|$:

$$n_0(\xi) = \frac{2L}{N}\int_{\xi}^{\xi_{max}} \frac{S(\xi_0)\,d\xi_0}{|v_x(\xi, \xi_0)|} \quad . \tag{8}$$

Here the upper integration limit is ξ_{max}, where ξ_{max} is the birth position farthest from ξ for which the ion does not turn around before reaching ξ; that is, for which v_x^2 above is non-negative. We assume that there is a sheath on the wall at $x = -L$ which reflects ions that would have reached the wall. The factor 2 in Eq. (8) accounts for the population of ions on the way back to their birth positions, having been turned around either by the sheath or by their Larmor gyrations. In relating to experimental results, the source $S(x)$ can be chosen so that the resulting density profile matches the measured one.

The average drift of the ion fluid $v_0(\xi)$, which is the same whether the ions are moving to the left or to the right, can be computed by a similar integration, but with the additional weighting factor $v_y(\xi, \xi_0)$, as given by Eq. (6):

$$v_0(\xi) = \frac{2}{n(\xi)}\int_{\xi}^{\xi_{max}} v_y(\xi, \xi_0)\,\frac{S(\xi_0)d\xi_0}{|v_x(\xi, \xi_0)|} \quad . \tag{9}$$

The integrations are easily performed, and the resulting profiles of n_0 and v_0 are shown in Ref. 4 for a uniform source, $S = 1$, and a Gaussian source, $S = \exp(-\xi^2)$. It is important to compute v_0 accurately because it is this small ion drift, not the much larger electron E × B drift, which matches the phase velocity of the unstable mode.

III. Radial wave equation

Since the first-order ion motions are small, the non-circular nature of the ion orbits in a sheared E-field can be neglected, and the ions can be treated as a cold fluid with the previously computed zero-order drift $v_0(x)$. The linearized ion equations of motion and continuity are simply

$$M\left(\frac{\partial \mathbf{v}}{\partial t} + \mathbf{v}_0 \cdot \nabla \mathbf{v} + \mathbf{v} \cdot \nabla \mathbf{v}_0\right) = e(\mathbf{E} + \mathbf{v} \times \mathbf{B}_0) \tag{10}$$

$$\frac{\partial n}{\partial t} + n_0 \nabla \cdot \mathbf{v} + \mathbf{v} \cdot \nabla n_0 + n \nabla \cdot \mathbf{v}_0 + \mathbf{v}_0 \cdot \nabla n = 0 \quad . \tag{11}$$

The electron fluid equations with finite E_0 and ∇n_0 yield the usual modified Boltzmann relation, which, for our $k_\parallel = 0$ case, simplifies to

$$\frac{n}{n_0} = \frac{e\phi}{KT_e} \frac{\omega_*(x)}{\omega - \omega_E(x)} \quad . \tag{12}$$

If k is the wavenumber in the y direction, the electron diamagnetic drift frequency ω_* is given by $-k(KT_e/eB_0)(n_0'/n_0)$, and the E × B drift frequency ω_E by $-kE_0/B_0$. For perturbations of the form $\phi = \phi(x)\exp(ky - \omega t)$, we can combine these three equations in straightforward fashion, keeping all x-derivatives ($'$) in both zero- and first-order quantities, to give the following differential equation for the fluctuating potential $\phi(x)$:

$$\phi'' + f(x)\,\phi' + g(x)\,\phi = 0 \quad . \tag{13}$$

Here the functions $f(x)$ and $g(x)$ are given by

$$f(x) = \delta(x) + \frac{2\omega_- k v_0' + \Omega_c v_0''}{\omega_-^2 - \Omega_c(\Omega_c + v_0')} \quad , \tag{14}$$

$$-g(x) = k\left[k + \frac{\Omega_c}{\omega_-} f(x) + \delta(x)\,\frac{\omega_-^2 - \Omega_c(\Omega_c + v_0')}{\Omega_c(\omega - \omega_E)}\right] \quad , \tag{15}$$

where

$$\omega_-(x) \equiv \omega - k v_0(x) \,, \qquad \delta(x) \equiv n_0'(x)/n_0(x) \quad . \tag{16}$$

The quantities n_0, v_0, ω_E, ω_-, and all their derivatives are functions of x, to be computed self-consistently as in Sec. II.

IV. Instability threshold

It will be convenient to use dimensionless units in which lengths are normalized to $L' \equiv L/N$ and frequencies to $\Omega_c = eB/M$, and thus velocities to $L'\Omega_c$. The dimensionless quantities (*) are then

$$
\begin{aligned}
x^* &= \xi = x/L', \quad & \omega^* &= \omega/\Omega_c, \quad & k^* &= kL', \quad & \delta^* &= \delta L' \\
v_0^* &= v_0/L'\Omega_c, \quad & \omega_-^* &= \omega^* - k^* v_0^*, \quad & c_S^2 &= KT_e/M, \quad & c_S^* &= c_S/L'\Omega_c \\
\omega_*^* &= -k^*\delta^* c_S^{*2}, \quad & n_0^* &= n_0 L'^3, \quad & S^* &= SL'^3/\Omega_c \quad .
\end{aligned}
\tag{17}
$$

As for the electrical quantities, since $e\phi/M$ is the square of a velocity, we can define a dimensionless ϕ^*, which is the square of v^*, as follows:

$$
\phi^* = \left(e/ML'^2\Omega_c^2\right)\phi, \qquad E^* = -\nabla^*\phi^* = \left(e/ML'\Omega_c^2\right)E \quad . \tag{18}
$$

The equilibrium profiles can then be written

$$
\begin{aligned}
\phi^* &= \phi_0^* \tanh\xi, \quad & E^* &= E_0^* \operatorname{sech}^2\xi, \quad & E_0^* &= -\phi_0^* \\
v_E^* &= -(E/B)/L'\Omega_c = -E_0^* \\
\omega_E^* &= k^* v_E^* = -k^* E_0^* \quad .
\end{aligned}
\tag{19}
$$

*From now on, we suppress the superscript * and assume that all quantities are in dimensionless form.*

In these units, Eqs. (13) to (15) become

$$
\phi'' + f(\xi)\phi' + g(\xi)\phi = 0 \tag{20}
$$

$$
f(\xi) = \delta + \frac{2\omega_- k v_0' + v_0''}{\omega_-^2 - (1 + v_0')} \tag{21}
$$

$$
g(\xi) = -k\left[k + \frac{f}{\omega_-} + \delta\,\frac{\omega_-^2 - (1+v_0')}{\omega - \omega_E}\right] \quad . \tag{22}
$$

The scaling of the eigenvalues of ω can be seen by making the local approximation $\phi' = \phi'' = 0$ and furthermore neglecting v_0' and v_0''. Eq. (20) then reduces to $g = 0$, or

$$
\omega_-^3 + (k/\delta)\left(\omega_-^2 - \omega_d\omega_-\right) - \omega_d = 0 \quad , \tag{23}
$$

where

$$
\omega_d \equiv k(v_E - v_0) \quad , \tag{24}
$$

ω_d being the difference between the electron and ion E-field drifts in the y direction. The cubic equation (23) has the standard form

$$
y^3 + py^2 + qy + r = 0 \quad , \tag{25}
$$

where $y = \omega - kv_0$, $p = k/\delta$, $q = -p\omega_d$, and $r = -\omega_d$. A complex conjugate pair of roots, one of which has $\mathrm{Im}(\omega) > 0$ and is therefore unstable, exists only if

$$
D \equiv (b/2)^2 + (a/3)^3 > 0 \quad , \tag{26}
$$

where

$$a = \frac{1}{3}(3q - p^2), \qquad b = \frac{1}{27}(2p^3 - 9pq + 27r) \quad . \tag{27}$$

The instability threshold, therefore, is given by $D = 0$. When $D > 0$, the unstable root is given by

$$\mathrm{Re}(\omega_-) = -\frac{1}{2}(A + B) - \frac{1}{3}p, \qquad \mathrm{Im}(\omega_-) = \frac{1}{2}\sqrt{3}\,|A - B| \quad , \tag{28}$$

where

$$A = \left(-\frac{1}{2}b + D^{1/2}\right)^{1/3}, \qquad B = \left(-\frac{1}{2}b - D^{1/2}\right)^{1/3} \quad . \tag{29}$$

When the magnetic field is sufficiently weak, the last term in Eq. (23) can be neglected, since it contains only one power of Ω_c in the denominator (when reconverted to dimensional units). In that case, the resulting quadratic equation yields the very approximate solution

$$\omega = kv_0 + \frac{1}{2}\,|k/\delta|\,\Omega_c + i(|k/\delta|\,\omega_d\,\Omega_c)^{1/2} \quad . \tag{30}$$

The second term in $\mathrm{Re}(\omega)$ is small whenever Ω_c is much smaller than ω. Then ω is approximately equal to kv_0, as observed [3], and is much smaller than ω_E, which it would be in the usual E × B instability.

We have computed the solution of Eq. (28) for $\phi_0 = 5\mathrm{V}$, $E = -10\mathrm{V/cm}$, and $k = 4$ cm^{-1}, which are the plane-geometry equivalents of the experimental parameters [3]. Using the equilibrium calculations of Sec. II for a Gaussian source, we find that $v_0 = 8 \times 10^4$ cm/sec and $\delta = -1.6$ cm^{-1} near the midplane. These values lead to $p = -2.5$, $q = 1610$, and $r = -644$ for the dimensionless parameters of Eq. (25). Fig. 2 shows the real and imaginary parts of $\omega - kv_0$ for the unstable root as functions of the normalized E × B drift frequency ω_E. It is seen that the frequency deviation from kv_0 remains nearly constant while the growth rate increases parabolically. There is a threshold around $\omega_E = 10$; at the experimental value of ≈ 600, the instability is well above threshold.

The instability boundary is plotted in Fig. 3 on the $k/|\delta|$ vs. normalized ω_d plane. The plasma is unstable except for large $|k|$ or small $|\delta|$, and there is a small region of stability for small ω_d which cannot be seen on this scale.

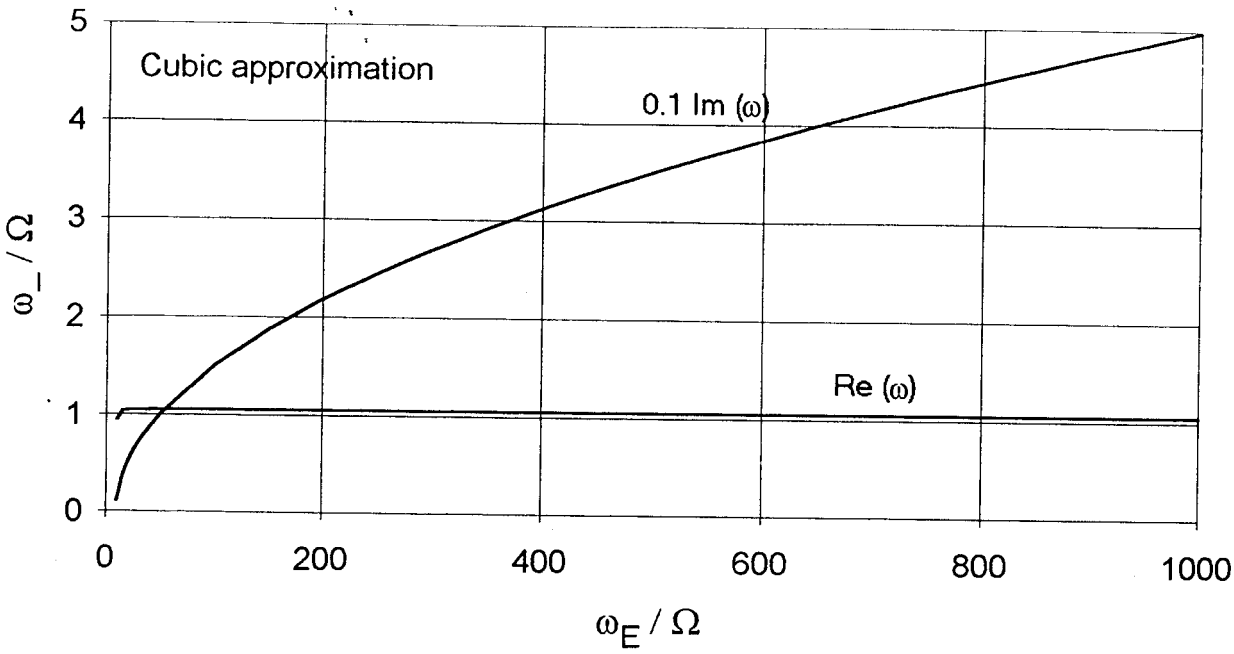

Figure 2: Frequency and growth rate vs. E × B drift frequency in the local approximation. Both are normalized to the ion cyclotron frequency. The frequency is given in the ion frame ($\omega_- = \omega - kv_0$), and the growth rate $\mathrm{Im}(\omega)$ has been reduced by a factor 10.

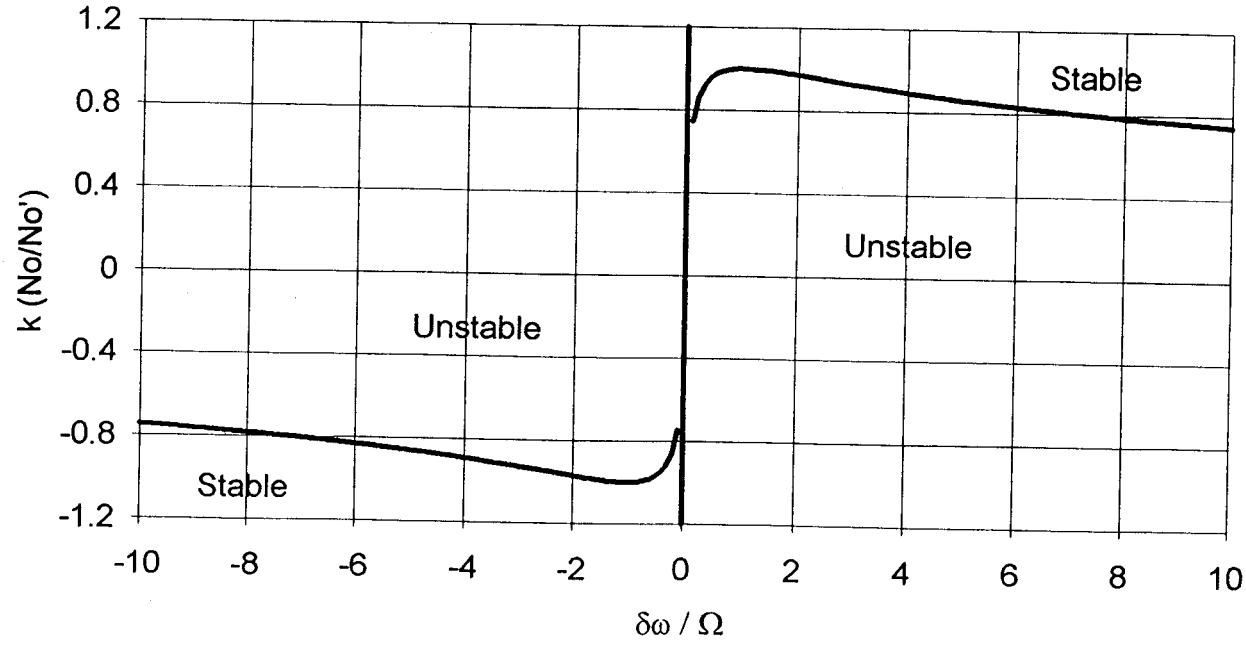

Figure 3: Stability boundaries as a function of the relative magnitudes and directions of the propagation constant k and the density gradient $\delta = n_0'/n_0$ on the one hand, and of the relative electron and ion fluid E × B drift speeds ($\delta\omega = \omega_E - kv_0$) on the other. A thin region of stability near $\delta\omega = 0$ cannot be seen on this scale.

V. Local dispersion relation

Having demonstrated that a strong instability is possible, we now investigate the detailed behavior of the instability. Since all of the quantities in Eqs. (20)-(22) except ω and k depend on ξ, the local value of ϕ will vary with position. There are two ways to compute the "local" dispersion relation: one is to neglect the derivatives of ϕ in Eq. (20), and the other is to first transform the equation to the WKB form $W'' + Q(x)\,W = 0$, and then to neglect W''. The difficulties we encountered were not sensitive to this choice, and we shall simply neglect ϕ' and ϕ'' in Eq. (20).

We first choose a Gaussian source function $S(\xi_0) \approx \exp(-\xi_0^2)$, with $N = 2$. Eqs. (8) and (9) then yield the n_0 and v_0 profiles shown in Fig. 4. Using a power-series fit to these profiles, and choosing a $\mathrm{sech}^2(\xi)$ profile for ω_E, we can then solve for $\omega(k)$ by setting $g(\xi) = 0$ in Eq. (22). This fifth-degree equation for complex ω was solved by iteration. Of the five roots, the unstable one that had $\omega \approx k v_0$ was picked out by starting the iteration from the desired root of the cubic equation (23), obtained by neglecting v_0' and v_0''. The resulting values of $\mathrm{Re}(\omega)$ and $\mathrm{Im}(\omega)$ as functions of ξ are shown in Fig. 5. It is seen that ω goes to infinity at $\xi \approx -1.6$. In this region, the solutions of the cubic and fifth-degree approximations also diverge from each other. Upon examination of the profiles of Fig. 4, we see that the density profile has a maximum at this position, so that the density gradient goes through zero there. The dip in density near the left boundary is to be expected, since many ions turn around before reaching the far left. When $\delta(\xi) = 0$ in Eq. (22), the fifth-degree equation becomes cubic, and two of the roots are lost. Apparently, these roots are lost by going to $\pm\infty$. The local value of ω, therefore, has no meaning in the neighborhood of a density extremum.

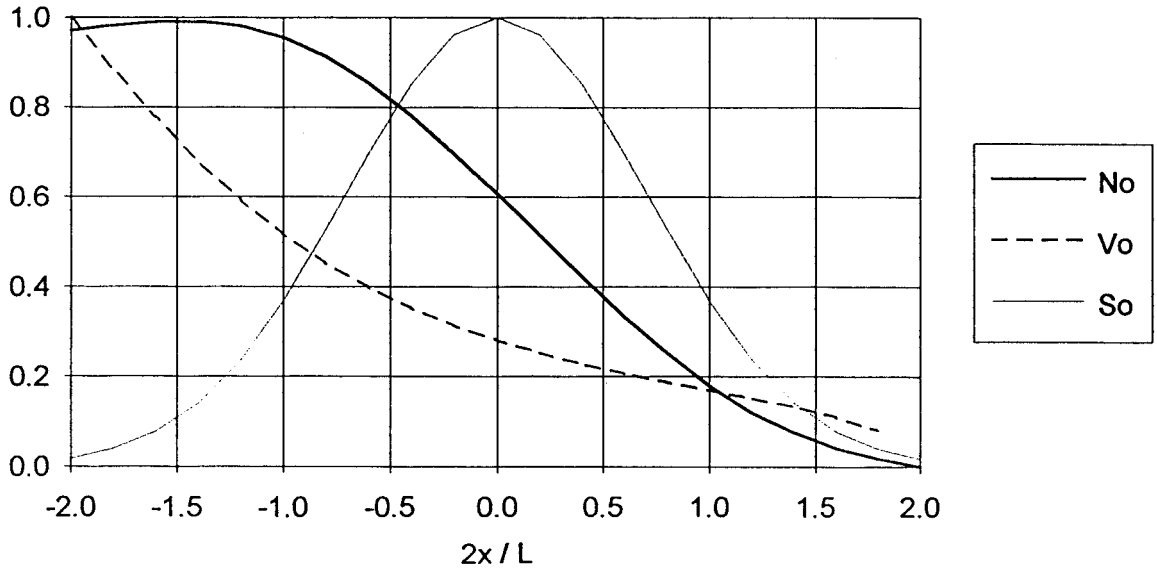

Figure 4: Equilibrium profiles of density n_0 and ion fluid y-velocity v_0 for a Gaussian source distribution S_0.

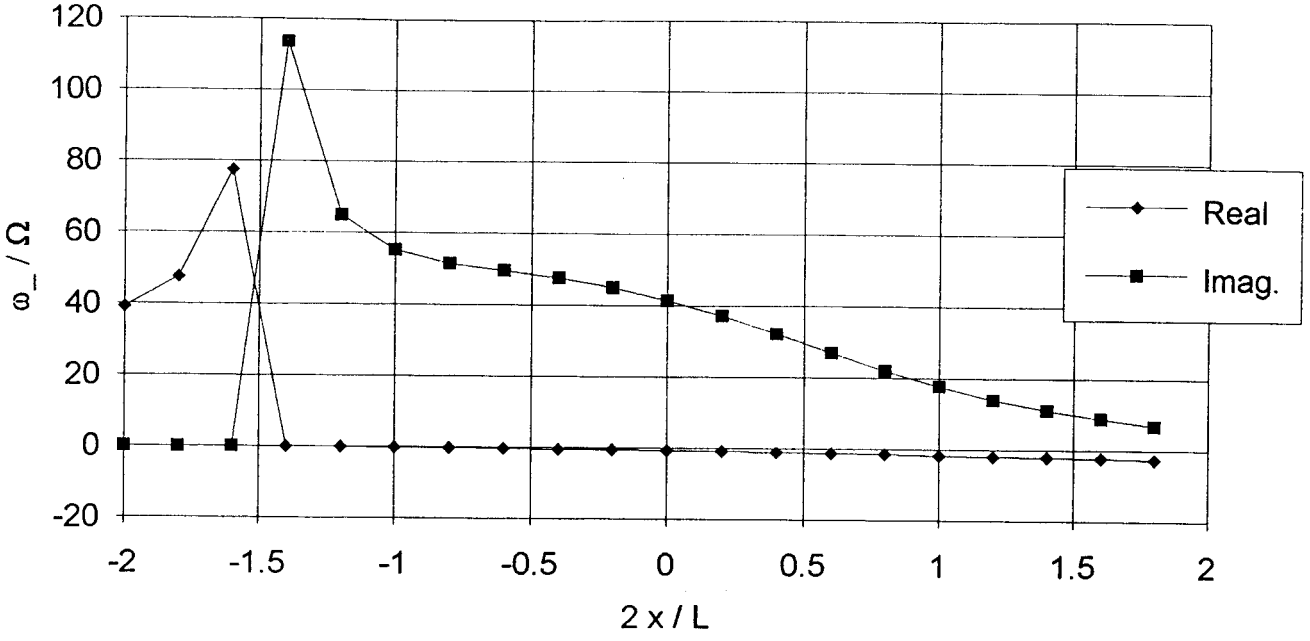

Figure 5: Local frequency and growth rate in the cubic approximation for a Gaussian source profile.

To remove this difficulty, we modified $n_0(\xi)$ by adding more particles near $\xi = -2$. Fig. 6 shows the n_0 and v_0 profiles produced by a bi-Gaussian source function $S(\xi_0) = \exp(-\xi_0^2/2.5)$ for $\xi < 0$ and $S(\xi_0) = \exp(-\xi_0^2/1.3)$ for $\xi > 0$. The density profile has been tailored to be nearly linear and monotonic, and the v_0 profile is still monotonic. The resulting local dispersion relation now appears reasonable, as shown in Fig. 7. The growth rate peaks in the region of largest E × B velocity, as one would expect. Furthermore, the cubic approximation (points) is in good agreement with the solution of the fifth-degree equation (line), showing that the shear terms v_0' and v_0'' in the ion fluid velocity are not important. Fig. 7 shows that the real part of $\omega - kv_0$ remains small, but the growth rate varies a factor of three over the width of the slab. To make a guess at the actual, global growth rate, we weighted the local growth rate by the local magnitudes of E, n_0, n_0', or n_0'/n_0. The weighted growth rates obtained this way ranged from 30 to 36 (except for the last case, which gave 20.5), as compared with a peak around 45 in Fig. 7. Such approximations, however, cannot be expected to be accurate in view of the unexpected shape of the perturbation found in the global solution of the next section.

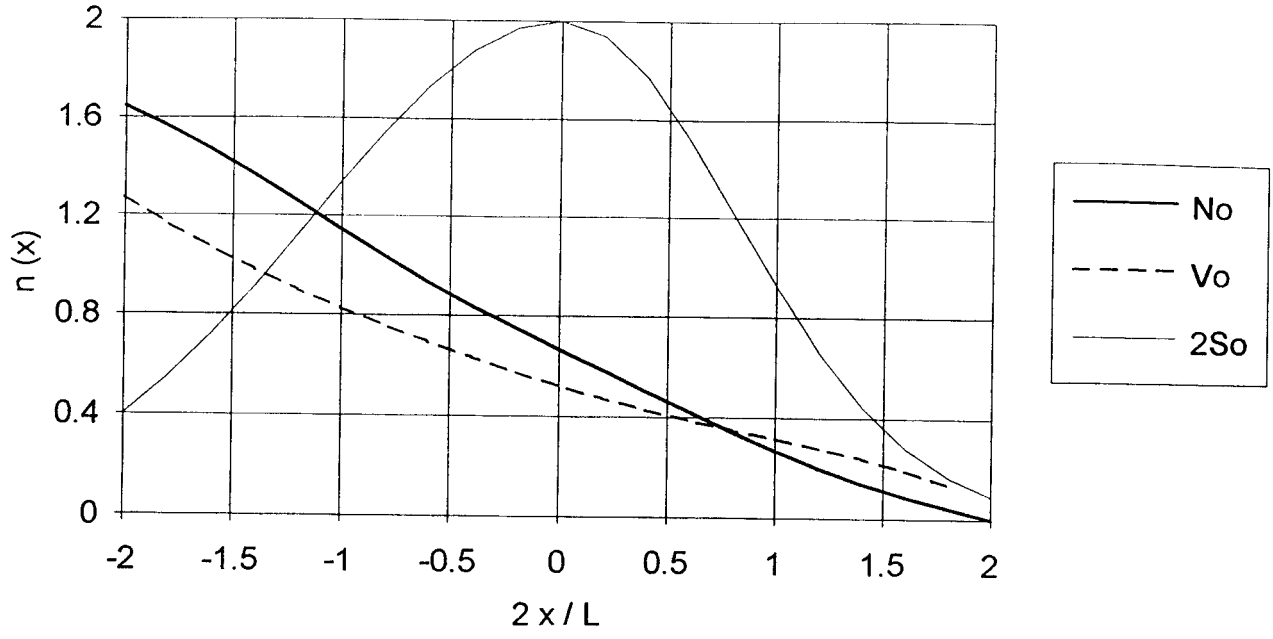

Figure 6: Equilibrium profiles of density n_0 and ion fluid y-velocity v_0 for a split Gaussian source distribution S_0 (also shown). The source has been chosen to yield a nearly linear density profile.

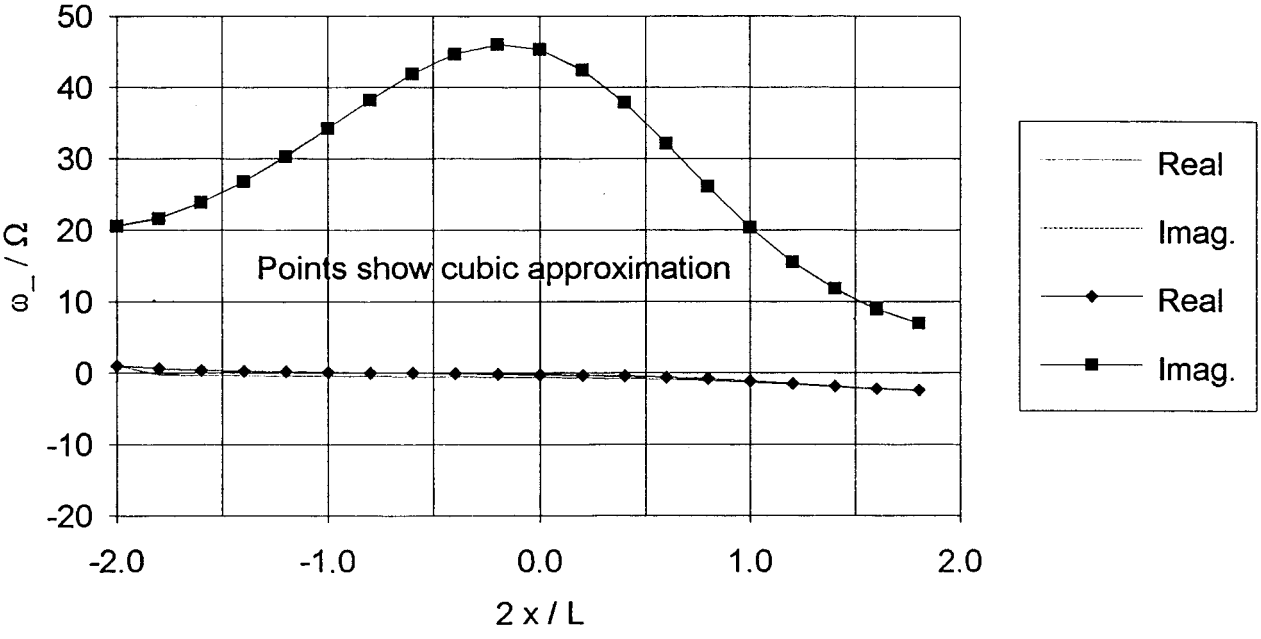

Figure 7: Local values of frequency and growth rate for the split Gaussian source profile. The points show the cubic approximation, and the lines are from the full fifth-degree equation, which includes the derivatives of v_0.

VI. Global eigenmodes

To find the dispersion relation accurately, we have integrated Eq. (20) numerically for the parameters listed above, using the local approximation as an initial guess for the complex value of ω. Since the value of $\delta(\xi)$ becomes infinitely large at the right boundary, where the density vanishes, we shot from the left boundary, with the initial values $\phi = 0$, $\phi' = 1$ at $\xi = -2$ $(x = L,\ N = 2)$, and complex ϕ is computed at each step using the local complex values of $f(\xi)$ and $g(\xi)$. The real and imaginary parts of ω are adjusted until both the real and imaginary parts of ϕ have their first zeroes at the right boundary, $\xi = 2$. The two-dimensional search for $\mathrm{Re}(\omega)$ and $\mathrm{Im}(\omega)$ is aided by the fact that $\mathrm{Re}(\omega - kv_0)$ is small for the root in question. These computations are simple enough to do on a personal computer. We have done them independently on a MacIntosh IIci using Fortran and a grid of 2000 points, and on a 486-50 PC using Excel 4.0 and a grid of 40 points. The results are in full agreement.

The eigenfunction $\phi(\xi)$ is shown in Fig. 8 for the nearly linear density profile of Fig. 6 and a $\mathrm{sech}^2(\xi)$ electric field profile. The values of $\mathrm{Re}(\omega)$ and $\mathrm{Im}(\omega)$ are reasonable, but somewhat larger than the local approximation would suggest. When a Gaussian source function is used, the eigenfunction, shown in Fig. 9, is almost the same in shape, but the value of ω is somewhat different. The reversal in slope of n_0' does not greatly affect the global mode, though it played havoc with the local solution. Note that $\mathrm{Im}\,\phi$ is always small. An x-variation of this quantity, corresponding to a radial variation in the cylindrical case, would have indicated an azimuthal phase that changes with radius; that is, a spiral perturbation. The eigenmode tends to be straight.

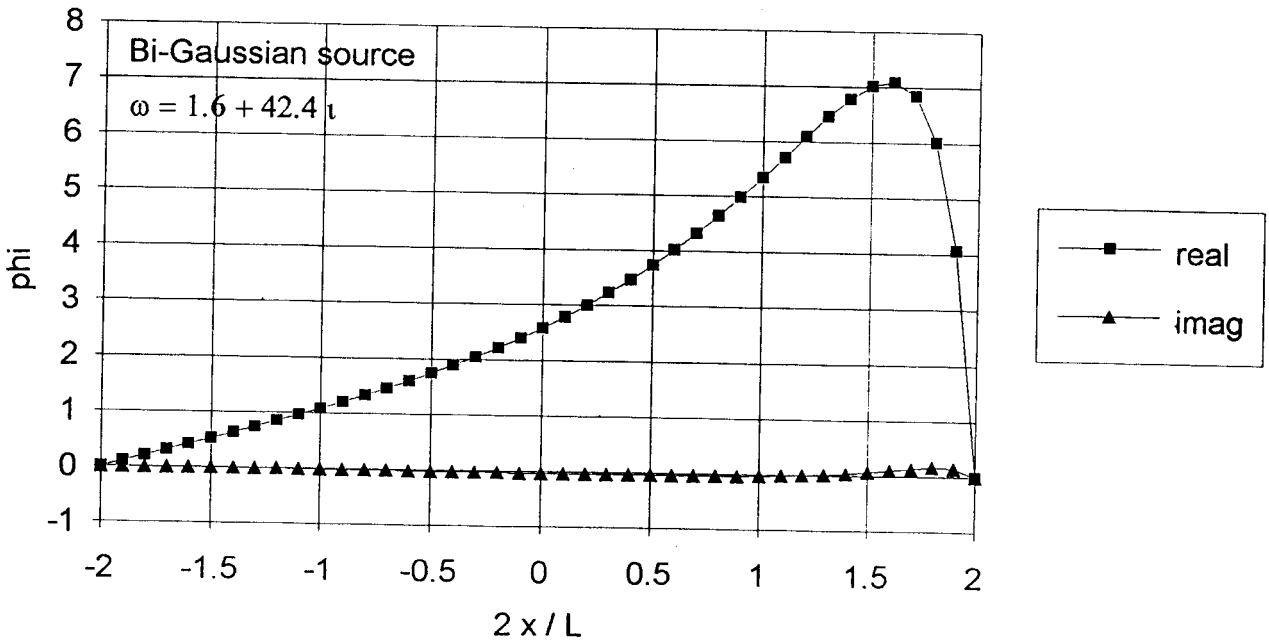

Figure 8: Real and imaginary parts of the lowest global eigenfunction ϕ for the bi-Gaussian source. The corresponding complex value of ω is also given.

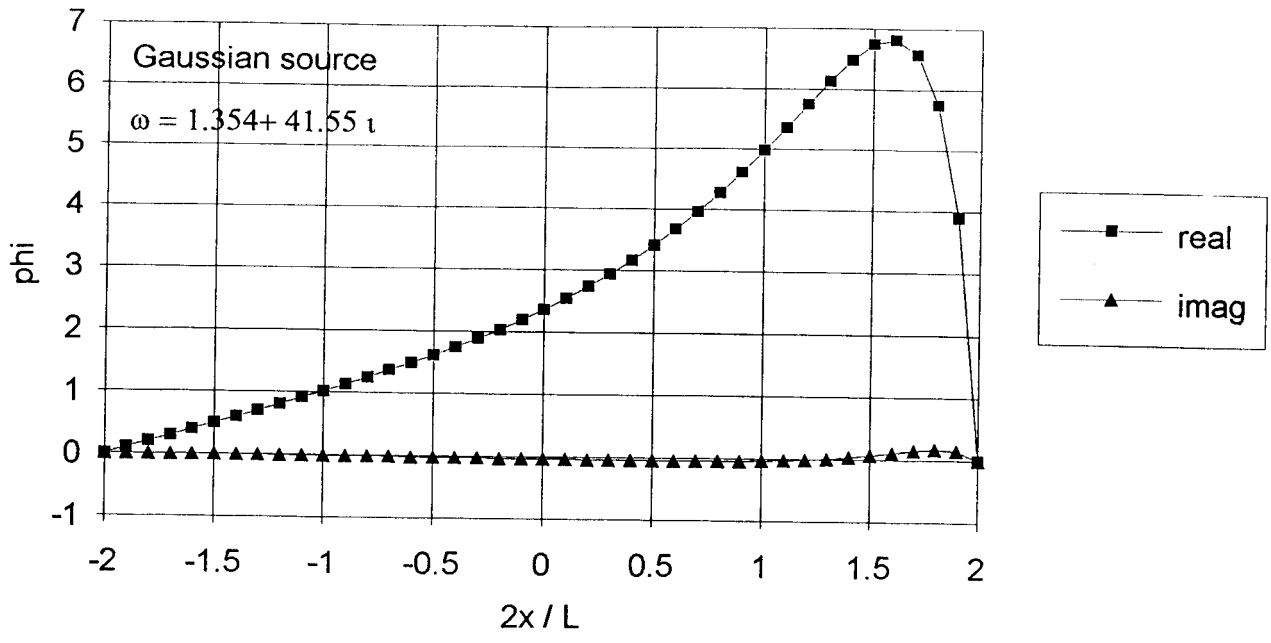

Figure 9: Same as Figure 8, but for a Gaussian source.

It was not expected that the perturbation would peak near the "outside" of the slab. The maximum in $\mathrm{Re}(\phi)$ occurs at a place where there is no peak in E_0, n_0, v_0, or any of their derivatives. To check that this effect is not a numerical error caused by the infinity in n_0'/n_0 near the right boundary, we repeated the shooting calculation, forcing the perturbation to vanish at $\xi = 1.9$, where the density is still finite. The result, shown in Fig. 10, yields a slightly different value of ω, but the shape of the eigenfunction is the same. We also tried shooting from the right, requiring ϕ to be zero at both boundaries. We could not let ϕ' be finite at $\xi = 2$, since $\delta(\xi)$ and hence $f(\xi)$ are infinite there, and thus ϕ'', computed from Eq. (20), would also be infinite. In this case, we took $\phi = \phi' = 0$, $\phi'' = 60$ at $\xi = 2$, giving a function $\phi(\xi)$ with about the same peak height as for the other cases. This is shown in Fig. 11. Now the value of ω is changed significantly, but the perturbation still peaks near the outside.

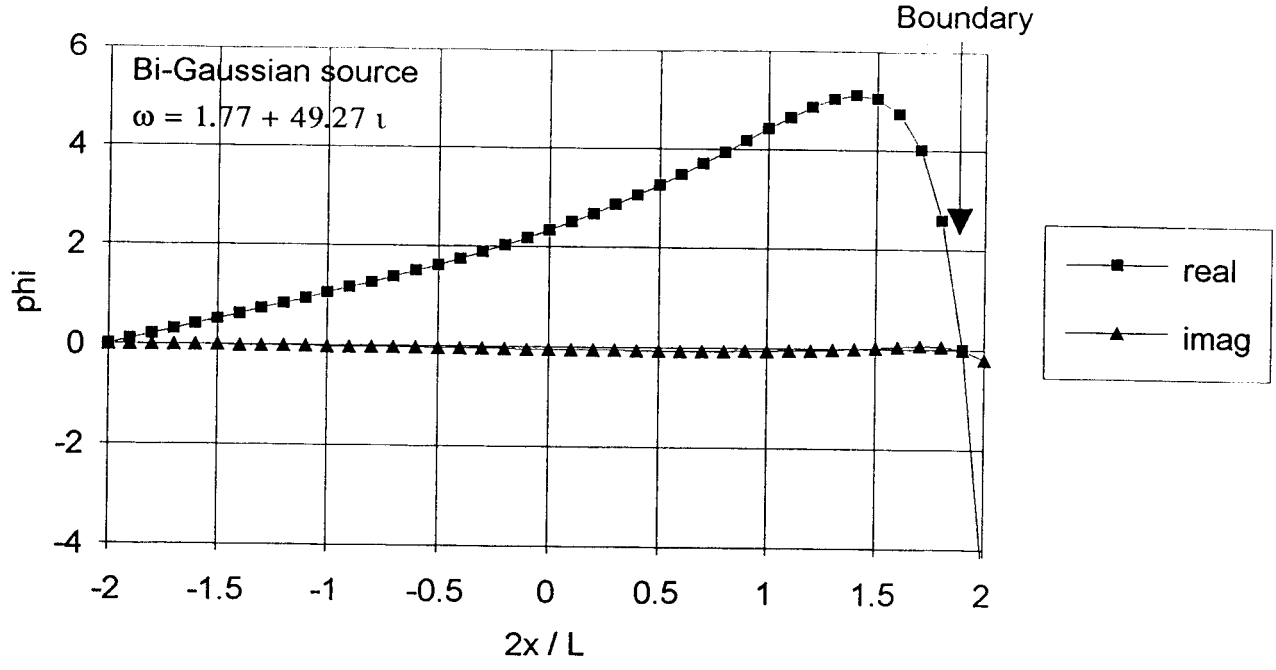

Figure 10: Same as Fig. 8, but the boundary where $\phi = 0$ has been taken at $\xi = 1.9$.

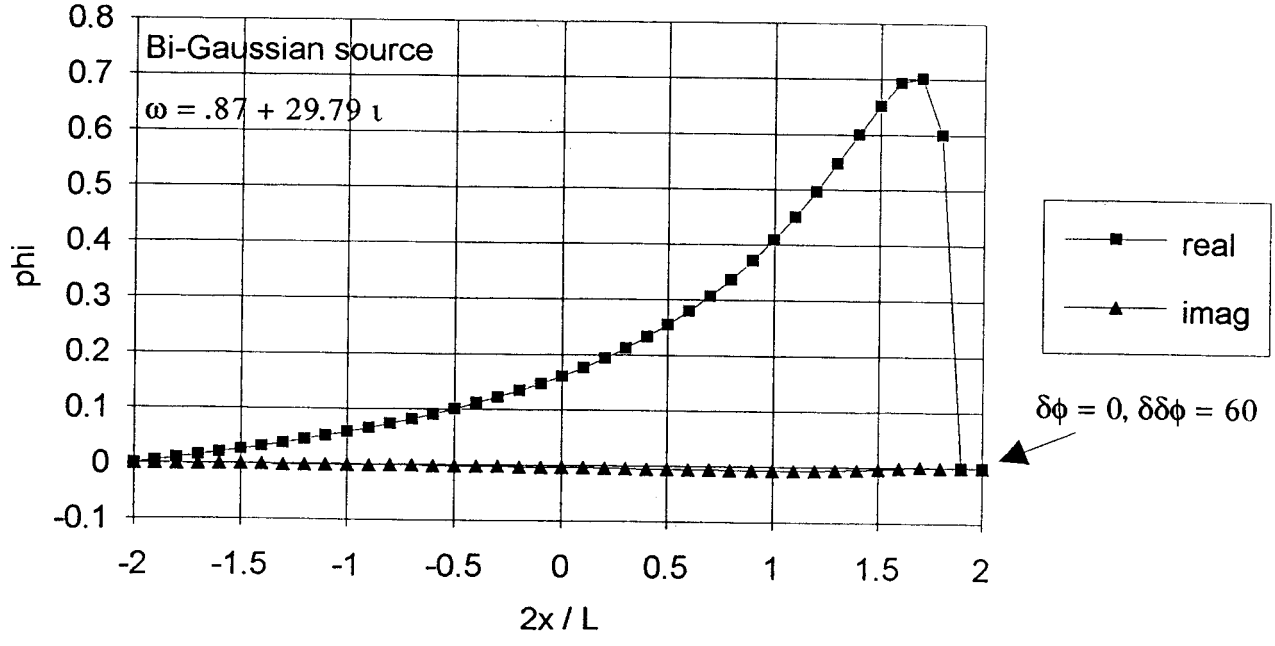

Figure 11: Same as Fig. 8, except that the integration was started from the right. The boundary condition there was taken to be $\phi = \phi' = 0$, $\phi'' = 60$.

Mathematically, the reason for this behavior is clear. Eq. (20) shows that ϕ'' is large wherever $\delta(\xi)$, and hence $f(\xi)$ and $g(\xi)$, are large. Since $\delta(\xi)$ has a sharp peak near the right boundary, $\phi(\xi)$ must have very large curvature there, even though it must go to 0 at $\xi = 2$. This can happen only if ϕ peaks just before boundary. The physical reason for this peaking is probably connected with the difference in ion and electron motions near the right boundary. As the wave field $\mathbf{E_1}$ passes by, the electrons move in the y direction in response to the component E_x. The ions, however, cannot follow them, since they have just been born and can be accelerated in the y direction only by the component $E_y = -ik\phi$, which is small there. A positive space charge then builds up, causing ϕ'' to be large. The resulting E_x drives the ions away from the region of excess ion space charge to preserve neutrality.

VII. Summary

We have given an example of a procedure by which the stability of a plasma against flute modes can be studied even when the zero-order electric field is highly sheared on the scale of the ion Larmor radius. Specifically, we have not assumed that the ion Larmor radius is smaller than the shear length. Kelvin-Helmholtz effects connected with the velocity shear of both the ions and electrons are included, and the density gradient is calculated self-consistently with these drifts. No drift wave effects appear because of the assumptions $k_\parallel = 0$ and $\omega \gg \Omega_c$. Using this formulation, experiments can be designed to investigate the stability of electric shear layers at the edge of a plasma, and the measurements analyzed theoretically in a fairly simple way which does not require extensive computations. For instance, the shear profile can be varied until stability is achieved, and the effects of the various derivatives of the electron and ion E $\times$ B profiles can be traced in the calculations.

This work was partially supported by NSF Grant No. ECS 89-01249 and by the University of Wisconsin Engineering Research Center. We are grateful to Dr. Y. Sakawa for access to his data.

References

1. A. Simon, *Phys. Fluids* **6**, 382 (1963).
2. F.C. Hoh, *Phys. Fluids* **6**, 1184 (1963).
3. Y. Sakawa, Thesis, UCLA, 1992; Sakawa et al., *Phys. Fluids* (to be published).
4. F.F. Chen, *Proc. 1992 Int'l Conf. on Plasma Physics* **III**, 1789 (Inst. for Ion Physics, Univ. of Innsbruck, A-6020 Innsbruck, Austria, 1992).